Stiffness of Optical Traps: Quantitative Agreement between Experiment and Electromagnetic Theory

Alexander Rohrbach

European Molecular Biology Laboratory, Meyerhofstrasse 1, 69117 Heidelberg, Germany

(Received 17 February 2005; published 13 October 2005)

The first quantitative agreement between measured and calculated stiffnesses of optically trapped particles in the subwavelength regime is presented. It is shown for all three dimensions that the measured extent of harmonic optical trapping potentials for dielectric spheres comes very close to the theoretically predicted extent, provided all known instrumental parameters are considered. The recently predicted strong asymmetry of the trapping potential due to the electric field's linear polarization has been verified in all three directions. This effect vanishes for spheres with diameters $d \approx \lambda$, which exhibit the strongest trap stiffnesses.

DOI: 10.1103/PhysRevLett.95.168102 PACS numbers: 87.80.Cc, 42.25.Fx, 42.30.Kq

Optical tweezers allow contactless holding and moving of particles in three dimensions [1] and have found broad applications in biophysics and colloidal sciences. Characterizing the optical trapping forces in the focus became necessary when small external forces had to be measured both in and far from equilibrium. Coherent light that is tightly focused with a standard microscope lens can generate a trapping potential $W(\mathbf{r})$, which is harmonic over a fraction of the trapping wavelength. In such a trap the linear restoring force $\partial_i W(x_i) \approx \kappa_i (x_i - x_{i0})$, in direction x_i, can be described by the force constant or stiffness κ_i ($i = x, y, z$ and $\partial_i = \partial/\partial x_i$). The optical force is zero at point x_{i0}. Although the potential is parabolic around x_{i0}, theories describing the correct trapping forces have failed. In a recent review it was stated [2]: "although the theory behind optical tweezers is still being developed, the basic principles are straightforward for objects either much smaller than the wavelength of light or much larger." It is curious that a physical theory agreeing with carefully measured data is still missing even considering that the most frequently used particle size is around the wavelength or slightly smaller.

The reasons for this are the large number of parameters describing the incident electromagnetic field, the interaction of this field with matter, and the method of how to measure trapping stiffnesses and forces. All relevant parameters must be taken into account both in a theory about trapping forces and in experiments. The necessity of reliable theories of optical trapping is underlined by the potential applications of optical trapping forces especially in nanotechnology, affecting manipulation, organization, process induction, and measurements of mesoscopic systems.

Various approaches using electromagnetic theories have been made to describe the trapping parameters of particles equal to or smaller than the trapping wavelength. These approaches are listed and described in Ref. [3] and only recently in Ref. [4]. However, besides our own work [3,5], only two studies used a realistic, aperture limited incident field [6,7] to calculate optical trapping forces. Most other studies were based on highly focused Gaussian beams ($\sin\alpha > 0.8$), which differ strongly [3] from a vectorial, diffraction limited focus as described by Richards and Wolf [8], and which are not a solution of the wave equation, i.e., therefore do not exist in nature.

Although the trap stiffness provides no information about the maximum trapping force or the depth of the trapping potential, it is an important parameter especially in Brownian systems. Via the equipartition theorem $\frac{1}{2} k_B T = \frac{1}{2} \kappa_i \langle x_i \rangle^2$ and the Einstein relation $\frac{1}{2} k_B T = \frac{1}{2} D \gamma$, the stiffness encodes information about fluctuation volumes $\langle x_i \rangle$, the diffusion constant D, or the viscous drag γ of a particle in a medium.

In this Letter, I compare theoretically and experimentally obtained trap stiffnesses for dielectric particles in the most frequently used size regime between 0.2 μm and 1.0 μm and with refractive indices $n_s = 1.43$ (silica) and $n_s = 1.57$ (polystyrene). The main parts of a theory, which is derived from the electromagnetic force density [9] and which is called the two-component approach, are reformulated and summarized.

Instrument.—An infrared corrected water immersion lens with a numerical aperture $\mathrm{NA} = n_m \sin\alpha = 1.2$ is used in our setup [10]. The refractive index of the medium (water) is $n_m = 1.33$ and the laser wavelength used is $\lambda_0 = 1.064$ μm in air ($\lambda = 0.8$ μm in water). The incident field, a Gaussian TEM_{00} mode of $\mathbf{E}_0 = E_0 \cdot \mathbf{e}_x$, is linear polarized in x and over illuminates the back focal plane (BFP) of the trapping lens by 200% (i.e., the Gaussian beam waist is 2 times the diameter D_{BFP} of the BFP). The aplanatic trapping lens fulfills the sine condition and leads to a spatially varying apodization at the BFP [3]. The transmission of the lens is $T = 62\%$ at $\lambda_0 = 1.064$ μm. Laser powers were measured behind the BFP [10].

Theory.—The electric field $\mathbf{E}_i(\mathbf{r})$ in the focus can be described as a composition of plane waves in the BFP with weighting factors $\tilde{\mathbf{E}}_i(k_x, k_y)$ (angular spectrum representation) [3]. In coherent optics the z component of the k vector is $k_z = \pm(k_n{}^2 - k_\perp{}^2)^{1/2} = k_n \cos\theta$, $k_\perp = (k_x{}^2 + k_y{}^2)^{1/2}$,

$k_0 = |\mathbf{k}_0| = 2\pi/\lambda_0 = k_n/n_m$. Therefore, the integral representing the field in the focus is only two dimensional:

$$\mathbf{E}_i(\mathbf{r}) = \frac{1}{(2\pi)^2} \iint_{k_\perp \le k_0 \mathrm{NA}} \tilde{\mathbf{E}}_i(k_x, k_y) \exp(-i\mathbf{k}\mathbf{r}) dk_x dk_y. \quad (1)$$

$\mathbf{E}_i(\mathbf{r})$ is the vectorial Fourier transform of the pupil function $\tilde{\mathbf{E}}_i(k_x, k_y)$ with radius $k_0\mathrm{NA} = k_n \sin\alpha$ considering the NA of the lens. The three components of $\tilde{\mathbf{E}}_i(k_x, k_y) = [\tilde{E}_{ix}(k_x, k_y), \tilde{E}_{iy}(k_x, k_y), \tilde{E}_{iz}(k_x, k_y)]$ are defined by a polarization function $\mathbf{P}(k_x, k_y)$ [11,12]. The modulus squares of the three components $|\mathrm{E}_{ix}|^2$, $|\mathrm{E}_{iy}|^2$, and $|\mathrm{E}_{iz}|^2$ add and result in an asymmetric focus distribution as shown in Fig. 1.

The total scattered field is obtained as follows: first, the spectrum $\tilde{\mathbf{E}}_s(k_x, k_y)$, resulting from the scattering of a single plane wave with amplitude E_0 and direction $\mathbf{k}_i = k_n \mathbf{e}_z$ at a sphere is calculated with Mie theory:

$$\tilde{\mathbf{E}}_s(k_x, k_y) = E_0 \cdot T_2(k_x, k_y) \cdot \frac{k_x}{k_n \cdot k_\perp^2} \cdot (k_x, k_y, -k_\perp^2/k_z) + E_0 \cdot T_1(k_x, k_y) \cdot \frac{k_x}{k_z \cdot k_\perp^2} \cdot (k_x, k_y, 0). \quad (2)$$

Here T_1 and T_2 are the angle-dependent Mie-scattering functions parallel and perpendicular to the plane of incidence [13]. In a next step, all other scatter spectra $\mathbf{M} \cdot \tilde{\mathbf{E}}_s(k_x, k_y)$ from the scattering of plane waves with amplitudes $\tilde{\mathbf{E}}_i(k_{ix}, k_{iy})$ and directions (k_{ix}, k_{iy}, k_{iz}) are obtained by multiplying Euler rotation matrices $\mathbf{M}(k_{ix}, k_{iy})$ [12]. All $\mathbf{M}(k_{ix}, k_{iy}) \cdot \tilde{\mathbf{E}}_s(k_x, k_y)$ with $k_{i\perp} < k_0\mathrm{NA}$ are superposed. The scattered field $\mathbf{E}_s(\mathbf{r}, \mathbf{b})$ at point $\mathbf{r}$ or its angular spectrum $\tilde{\mathbf{E}}_s(k_x, k_y, \mathbf{b})$ change with the particle position $\mathbf{b}$ relative to the center of the focus.

Trapping forces are derived from the Lorentz force density $\mathbf{f} = (\mathbf{p}\nabla\mathbf{E}) + \partial\mathbf{p}/\partial t \times \mathbf{B}$ for dipoles, where a linear response on the total electric field $\mathbf{p}(\mathbf{r}, t) = \alpha_0 \cdot \varepsilon\mathbf{E}(\mathbf{r}, t)$ is assumed. Higher polarization moments are neglected, which is valid for reasonable laser powers and the specified particle sizes. $\mathbf{E}(\mathbf{r}, t)$ and $\mathbf{B}(\mathbf{r}, t)$ are the total electric and magnetic field, respectively. The polarizability on a volume element V is $\alpha_0 = 3V\ (m^2 - 1)/(m^2 + 2)$, where $m = n_s/n_m$ is the ratio of the refractive indices of the scatterer and the surrounding medium and $\varepsilon = {n_m}^2\varepsilon_0$ is the electric permittivity [14]. After integrating the time-averaged force density $\langle f(\mathbf{r}, \mathbf{b})\rangle = \mathrm{Re}\{\alpha_0\varepsilon\nabla|E(\mathbf{r}, \mathbf{b})|^2\}/4V$ over the volume of the scatterer at position $\mathbf{b}$, one obtains the expression of the optical force without the detour of the Maxwell stress tensor [9]:

$$\begin{aligned}\mathbf{F}(\mathbf{b}) &= \frac{1}{4V}\,\mathrm{Re}\int_V \alpha_0\varepsilon\nabla|\mathbf{E}_i + \mathbf{E}_s(\mathbf{b})|^2 dV \\ &= \frac{1}{4V}\,\mathrm{Re}\int_V \alpha_0\varepsilon\nabla|\mathbf{E}_i|^2 dV \\ &\quad + \frac{1}{4V}\,\mathrm{Re}\oint_{\partial\mathrm{V}} \alpha_0\varepsilon\mathbf{n}[\mathbf{E}_i^*\mathbf{E}_s(\mathbf{b}) + \mathbf{E}_i\mathbf{E}_s^*(\mathbf{b}) \\ &\quad + |\mathbf{E}_s(\mathbf{b})|^2] dA. \end{aligned} \quad (3)$$

The force is split into two components, the gradient force and the scattering force, resulting from the incident and the scattered field, $\mathbf{E}_i$ and $\mathbf{E}_s$. The scattering force (described by the surface integral) results from the extinction and redistribution of momentum. For dielectric particles in the Rayleigh-Gans regime (also known as Born approximation), the following expression for the two force components is valid [14]:

$$\begin{aligned}\mathbf{F}(\mathbf{b}) &= \mathbf{F}_{\mathrm{grad}}(\mathbf{b}) + \mathbf{F}_{\mathrm{sca}}(\mathbf{b}) \\ &\approx \frac{\alpha_0 n_m}{2cV}\int_{V(b)} \nabla I_0(\mathbf{r}) d^3r \\ &\quad + \frac{n_m}{kc} I_0(\mathbf{b})[C_{\mathrm{ext}}(\mathbf{b})\langle\mathbf{k}_i(\mathbf{b})\rangle - C_{\mathrm{sca}}(\mathbf{b})\langle\mathbf{k}_s(\mathbf{b})\rangle]. \end{aligned} \quad (4)$$

The space-variant gradient ∇I_0 of the incident intensity $I_0(\mathbf{r}) = c\varepsilon/2|\mathbf{E}_i(\mathbf{r})|^2$ is averaged over the particle volume in real space. With this first-order Born approximation one avoids the elaborate calculation of the electric fields on the surface of the scatterer or the exact internal fields. The second term in Eq. (4) describes the extinction and redistribution of momentum, given by the cross sections $C_{\mathrm{ext}} = C_{\mathrm{sca}} = Q_{\mathrm{sca}}\pi(d/2)^2$ together with the mean momentum vectors $\langle\mathbf{k}_i\rangle$ and $\langle\mathbf{k}_s\rangle$ of the incident and scattered fields, respectively [3]. They are all functions of the far-field spectra $\tilde{\mathbf{E}}_{\mathrm{ext}}(k_x, k_y, \mathbf{b}) = \mathrm{FT}\{\mathbf{E}_i(x, y, b_z)q(x - b_x, y - b_y)\}$ for extinction and $\tilde{\mathbf{E}}_s(k_x, k_y, \mathbf{b})$ for scattering, (FT = Fourier transform). $q(x, y)$ is an extinction function removing the fraction Q_{sca} from the incident intensity $|\mathbf{E}_i(x, y, b_z)|^2$ at the position (b_x, b_y) of the scatterer, $[q(x, y)]^2 = 1 - Q_{\mathrm{sca}}\theta(d/2 - r)$, $r = (x^2 + y^2)^{1/2}$, $\theta(r) =$ Heaviside step function.

Finally, the force constants κ_i at the trapping position $(0, 0, z_0)$ are obtained according to $\kappa_i = \partial_i F_i(x_i)|_{x_{i0}} = \partial_i[F_{i,\mathrm{grad}}(x_i) + F_{i,\mathrm{sca}}(x_i)]|_{x_{i0}}$. The calculation results point out that in lateral direction $\partial_i F_{i,\mathrm{grad}}$ and $\partial_i F_{i,\mathrm{sca}}$ have opposite signs, whereas in axial direction they have the same sign. Therefore, the scattering force decreases the trap stiffness in lateral direction, but increases the stiffness in axial direction [see, e.g., Fig. 5 of [3]].

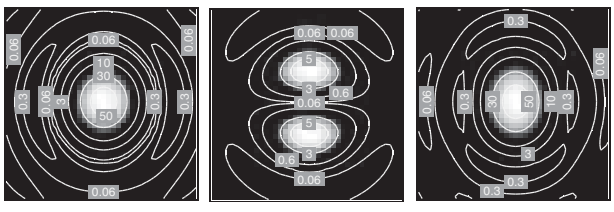

FIG. 1. Asymmetric intensity distribution $I(x, y, z = 0)$ in the focal plane for linear polarized light and NA = 1.2. The sum of the intensities of $|E_x|^2$ (left) and $|E_z|^2$ (center) is $I = I_x + I_z$ (right). The negligibly small component I_y is not shown. The extents of the plots are 2λ by 2λ.

Experiments.—The three-dimensional position signals $S_i(x_i)$ $(i = 1, 2, 3)$ of various trapped particles at various laser powers were tracked with back-focal-plane interfer-

ometry [15]. 400 000 positions were recorded at 100 kHz. The signals $S_i(x_i) = g_i x_i$ are linear with the displacement x_i over a sufficiently large range. The signal autocorrelations $\langle S_i(t)S_i(t+\tau)\rangle = \langle |S_i(0)|^2\rangle \exp(-\tau\kappa_i/\gamma)$ provide the autocorrelation times τ_i, i.e., the stiffnesses $\kappa_i = \gamma/\tau_i$ for known viscous drag $\gamma = 3\pi d\eta$ (d = sphere diameter, η = viscosity, $\eta(T = 295\ \mathrm{K}) = 950\ \mu\mathrm{Pa}\cdot\mathrm{s}$). Glass spheres with refractive index $n_s = 1.43$ and mean diameters $d = 0.64\ \mu$m and $d = 1\ \mu$m were used as well as polystyrene (PS) spheres with $n_s = 1.57$ and $d = 0.216\ \mu\mathrm{m} \ldots 1.66\ \mu$m. All spheres are from Bangs Labs Inc., except for the fluorescence labeled $0.216\ \mu$m, $1.03\ \mu$m, and $1.66\ \mu$m beads (Polysciences, Inc.). Laser powers were varied between 4.8 mW and 48 mW. For each particle type about 50 measurements on three particles were performed and analyzed.

Results.—Figure 2 shows the expected linear dependency between trap stiffnesses and laser power. But, and this has never been shown before, the trap reveals a strong asymmetry also in lateral direction, which is due to the electric field's linear polarization. This difference in the lateral trap stiffness was strongly reduced by inserting a quarter wave plate (the light remained slightly elliptically polarized due to polarization dependent dichroic mirrors). The triplet of measured trap stiffnesses $\{\kappa_x, \kappa_y, \kappa_z\}$ is summarized in Table I for all particles investigated, whereas Table II shows the different ratios of trap stiffnesses. The lateral stiffnesses κ_x and κ_y are calculated at the predicted axial trapping position z_0 according to $\kappa_i = \partial_i F_i(x_i)|_{z0}$.

Figure 2 also demonstrates the accuracy of the theoretically predicted stiffnesses (lines) for the three smaller spheres ($d = 0.22$, 0.53, and $0.64\ \mu$m), which show an unequaled agreement with the experimental values (symbols). In lateral directions the difference between theory and experiment is 2%–6%; in axial directions it is 10%–30% depending on the sphere size. For the larger particle in Fig. 2 with $d = 0.85\ \mu$m and central phase shift $\Delta\phi = (n_s - n_m)k_0 d = 1.2$ the trap is nearly symmetric in x and y, whereas the calculated results yield a (modest) asymmetry. Here the size and phase shift are beyond the Born approximation used in Eq. (4). For the $1.03\ \mu$m PS sphere κ_x and κ_y were not calculated at the predicted position $z_0 < 0$, but at the likely position $z_0 = 0.1\ \mu$m.

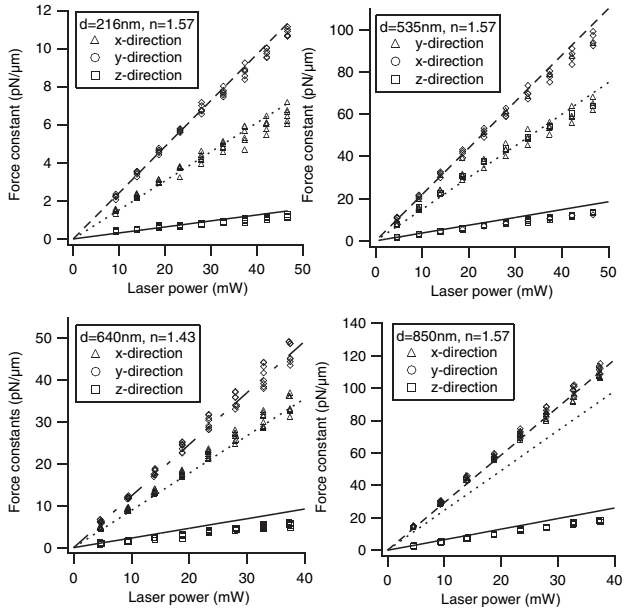

FIG. 2. Trap stiffnesses along x, y, and z as a function of laser power in an x-polarized beam. The symbols correspond to experimental data, whereas the lines describe the theoretical force constants.

Figure 3 summarizes the results of the comparison between electromagnetic theory and experiment for PS spheres, showing the normalized stiffness per unit laser power as a function of the sphere's diameter. κ_x and κ_y increase with the sphere diameter d until d reaches the expected lateral extent of the focus $\delta_y(I_0/e^2) \approx 0.8\Delta_y \approx \lambda$ with $\lambda = 0.8\ \mu$m. $\delta_y(I_0/e^2)$ is the width where the focus intensity decreases to $1/e^2$ of the maximum intensity I_0. We expect the same behavior for the axial stiffness κ_z at a theoretical axial focus extent of $\Delta_z \approx 2.3\Delta_y$ [16]. κ_x and κ_y fall off again for diameters $d > \delta_y$. The same nonlinear behavior is predicted by the theory as shown in Fig. 3 and Table I (for the $1.66\ \mu$m bead we solely calculated the gradient force). At the same time, a vanishing asymmetry of the trap due to polarization at $d \approx \lambda = 0.8\ \mu$m was measured. This asymmetry effect is confirmed by the calculations. Table II shows the relative trapping stiffnesses for both theory and experiment. It can be further seen that a trapping potential becomes less prolate in axial direction with increasing sphere size; i.e., the ratio of trapping stiffnesses κ_{xy}/κ_z decreases. The ratios $\kappa_{xy}/\kappa_z = 7$ and $\kappa_{xy}/\kappa_z = 4$ are illustrated by the measured position traces of a $0.22\ \mu$m bead and a $1.03\ \mu$m bead in the right-hand side of Fig. 3.

Conclusions.—It has been shown for the first time that results from an electromagnetic theory of optical trapping forces considering all known relevant parameters are in very good agreement with experimental results for spheres

TABLE I. Sphere parameters and measured trapping stiffnesses at a laser power of $P = 10$ mW in the focal plane. D is the mean sphere diameter in μm, n_s the spheres refractive index, $\Delta\phi = (n_s - n_m)k_0 d$ the central phase shift; κ_x, κ_y, and κ_z are the measured trap stiffnesses in pN/μm.

D	n_s	$\Delta\phi$	κ_x	κ_y	κ_z
0.22	1.57	0.31	1.46	2.36	0.27
0.53	1.57	0.76	14.6	21.1	2.91
0.69	1.57	0.98	24.2	26.5	4.29
0.85	1.57	1.20	29.4	30.4	5.03
1.03	1.57	1.46	28.2	25.2	6.20
1.66	1.57	2.35	11.0	10.0	3.85
0.64	1.43	0.38	9.45	12.6	1.58
1.00	1.43	0.59	10.6	10.0	2.91

TABLE II. Sphere parameters and relative trapping stiffnesses. $1 - \kappa_x/\kappa_y$ is the difference in lateral stiffness illustrating the polarization effect; $\kappa_{xy}/\kappa_z = (\kappa_x + \kappa_y)/2\kappa_z$ is the ratio between mean lateral and axial stiffness.

		$1 - \kappa_x/\kappa_y$		κ_{xy}/κ_z	
D	n_s	Theory	Experiment	Theory	Experiment
0.22	1.57	0.37	0.38	6.5	7.1
0.53	1.57	0.32	0.31	5.0	6.1
0.69	1.57	0.33	0.08	4.7	5.9
0.85	1.57	0.16	0.03	4.2	5.9
1.03	1.57	0.05	−0.12	3.8	4.3
1.66	1.57	(0.10)	−0.10	(2.1)	2.7
0.64	1.43	0.28	0.25	4.6	7.0
1.00	1.43	0.02	−0.06	3.3	3.5

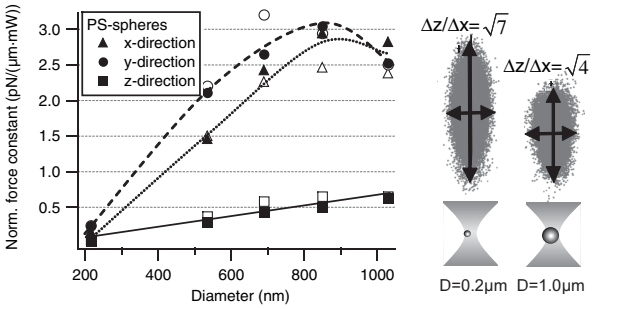

FIG. 3. Change of the force constant per unit laser power for various polystyrene spheres ($\lambda = 800$ nm in water). White markers indicate theoretical values, black markers experimentally obtained stiffnesses, experimental error bars are all below 1%. The lines are drawn to guide the eye. Right: the trapping volumes of a 0.22 μm and 1.03 μm bead indicate the different ratios of axial to lateral stiffness.

with diameters $d < \lambda$ and in good agreement for spheres $d \approx \lambda$. The lateral trap stiffnesses κ_i, and with them the extents $\langle x_i \rangle$ of the trapping potentials, differ strongly in lateral directions due to the electric field's polarization. This effect vanishes as d reaches the lateral focus extent. At this diameter the maximum lateral trapping stiffness is also achieved. A third effect coupled to the first two is that the size of the trapped sphere determines the aspect ratio of the trapping potential; i.e., the stiffness ratio κ_{xy}/κ_z decreases for larger spheres.

These three observations can be interpreted by means of the two components force approach as follows: first, the lateral gradient force $F_{\perp,\mathrm{grad}}(x_\perp)$ and therefore the gradient $\partial_\perp F_{\perp,\mathrm{grad}}(x_\perp)$ are reduced by averaging the intensity gradients over sphere volumes larger than the dimensions of the focus ($\partial_\perp F_{\perp,\mathrm{grad}}$ reaches a maximum). Second, the repelling lateral scattering force $F_{\perp,\mathrm{sca}} > 0$ increases for larger spheres and compensates the attractive $F_{\perp,\mathrm{grad}} < 0$ such that $\kappa_\perp = \partial_\perp F_{\perp,\mathrm{sca}} + \partial_\perp F_{\perp,\mathrm{grad}}$ decreases. Third, the radiation pressure (axial scattering force $F_{z,\mathrm{sca}}$) increases with the sphere size and therefore amplifies the axial trap stiffness $\kappa_z = \partial_z F_{z,\mathrm{grad}}(z) + \partial_z F_{z,\mathrm{sca}}(z)$ at the trapping position z_0 ($\partial_z F_{z,\mathrm{grad}}$ and $\partial_z F_{z,\mathrm{sca}}$ have the same sign).

I state that the Born approximation (which is used to determine $\mathbf{F}_{\mathrm{grad}}$) delivers reasonable results even for a central phase shift $\Delta\phi > 1$ in the case of highly focused fields. Although $\mathbf{F}_{\mathrm{grad}}$ plays a dominant role for optical trapping of subwavelength particles, the effect of $\mathbf{F}_{\mathrm{sca}}$ for spheres with $\Delta\phi \approx 1$ and with diameters close to the trapping wavelength cannot be neglected [as was done by Tlusty *et al.* [17]]. They obtained a satisfying coincidence between theory and experiment in one lateral dimension, although they used arguable approximations concerning the particle and the focused beam. The good coincidence between our theory and experiments would not have been possible without the influence of $\mathbf{F}_{\mathrm{sca}}$ and the realistic description of the incident focused field. This was inspected by looking at the stiffnesses solely obtained by $\mathbf{F}_{\mathrm{grad}}$. The need to calculate the redistribution of momentum via $\mathbf{F}_{\mathrm{sca}}$ is underlined by the fact that the scattered light delivers the exact position of the particle inside the trap [12].

I believe that this study delivers an important contribution towards a better understanding and optimization of optical trapping forces for subwavelength sized particles.

I thank Dr. Ernst Stelzer for general support, Peter Seitz and Alfons Riedinger for the development of the automation software, and Holger Kress and Dr. Jim Swoger for helpful discussions.

[1] A. Ashkin *et al.*, Opt. Lett. **11**, 288 (1986).
[2] D. G. Grier, Nature (London) **424**, 810 (2003).
[3] A. Rohrbach and E. H. K. Stelzer, J. Opt. Soc. Am. A **18**, 839 (2001).
[4] K. C. Neuman and S. M. Block, Rev. Sci. Instrum. **75**, 2787 (2004).
[5] A. Rohrbach and E. H. K. Stelzer, Appl. Opt. **41**, 2494 (2002).
[6] K. Visscher and G. J. Brakenhoff, Optik (Jena) **89**, 174 (1992).
[7] D. Ganic, X. Gan, and M. Gu, Opt. Express **12**, 2670 (2004).
[8] B. Richards and E. Wolf, Proc. R. Soc. London, Ser. A **253**, 358 (1959).
[9] J. D. Jackson, in *Classical Electrodynamics* (Wiley, New York, 1975).
[10] A. Rohrbach *et al.*, Rev. Sci. Instrum. **75**, 2197 (2004).
[11] M. Mansuripur, J. Opt. Soc. Am. A **3**, 2086 (1986).
[12] A. Rohrbach and E. H. K. Stelzer, J. Appl. Phys. **91**, 5474 (2002).
[13] H. C. van de Hulst, *Light Scattering by Small Particles* (Dover, New York, 1957).
[14] A. Rohrbach, H. Kress, and E. H. K. Stelzer, Appl. Opt. **43**, 1827 (2004).
[15] A. Pralle *et al.*, Microsc. Res. Tech. **44**, 378 (1999).
[16] According to Ernst Abbe one expects $\Delta_y = 1.2\lambda_0/(n_m \sin\alpha)$ and $\Delta_z = 2\lambda_0/(n_m - n_m \cos\alpha)$.
[17] T. Tlusty, A. Meller, and R. Bar-Ziv, Phys. Rev. Lett. **81**, 1738 (1998).